J. Plasma Physics (1998), *vol.* 60, *part* 1, *pp.* 81–93. Printed in the United Kingdom

© 1998 Cambridge University Press

The double sheath associated with electron emission into a plasma containing negative ions

H. AMEMIYA,[1] B. M. ANNARATONE[2] and J. E. ALLEN[2]

[1] The Institute of Physical and Chemical Research, Hirosawa, Wako, Saitama-Prefecture, Japan 351-01
[2] Department of Engineering Science, University of Oxford, Parks Road, Oxford OX1 3PJ, UK

(Received 4 June 1997 and in revised form 7 November 1997)

The double sheath formed by thermal electrons and negative ions in a plasma and electrons emitted from an electrode is investigated. The ion energy at the sheath edge and the electric field at the electrode surface are calculated for several values of the ratio of negative-ion density to electron density. The maximum beam density above which a virtual cathode appears is given. The relation to the Langmuir limit is shown. The numerical results for the electric potential, the electric field and the space charge density are presented. The floating potential is calculated from the current balance of all components.

1. Introduction

Since the original work of Langmuir (1929), double-layer phenomena have been treated by many authors. Of these, the case with electron emission is of current interest from the viewpoint of the control of the potential of a substrate immersed in a reactive plasma. A sheath and presheath with electron emission have been considered in a hot plasma (Hobbs and Wesson 1967). Above a critical value of the emission rate, the sheath becomes a double sheath. A criterion for the formation of a double sheath associated with a hot cathode immersed in a plasma was considered by Prewett and Allen (1976). Double layers (or sheaths) between two plasmas have been studied by Andrews and Allen (1971), Levine and Crawford (1980), and others.

The present work is an extension of a previous double layer theory (Prewett and Allen 1976) to the case with negative ions. The case with negative ions is considered to be important for the potential control of an electrode in etching and deposition plasmas as well as the extraction electrode of a negative-ion source.

2. Model

Figure 1 shows a one-dimensional model that extends that of Prewett and Allen (1976) to the case with negative ions. From the right-hand side of the sheath edge, thermal electrons and negative ions penetrate the sheath, following Boltzmann distributions. Positive ions flow toward the substrate. An electron beam is ejected from the left-hand electrode, which may be a cathode or a substrate, towards the plasma. The beam is assumed to be monoenergetic.

https://doi.org/10.1017/S0022377898006837 Published online by Cambridge University Press

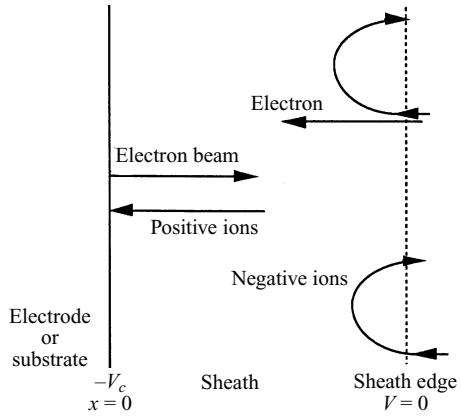


Figure 1. Schematic diagram of the model.

The following nomenclature is employed: the electron, positive and negative ion densities at the sheath edge are n_{e0}, n_{i0} and n_{n0}; the potential in the sheath is $-V$, the plasma potential is $V = 0$ and the electrode potential is $-V = -V_c$; the initial velocity of positive ions entering the sheath is v_0; the electron and negative-ion temperatures are T_e and T_n; and the electronic charge and mass are e and m.

The density n_b of electrons produced by thermionic emission or secondary emission, which form an electron-beam current j_b, is given, in the absence of ionization in the sheath, by

$$n_b = \frac{j_b}{e}\left(\frac{m}{2e}\right)^{1/2}(V_c - V)^{-1/2}. \tag{1}$$

This model assumes monoenergetic ions. The positive ions enter the sheath with initial energy $\frac{1}{2}Mv_0^2$, the equivalent potential drop being V_0. The flux of ions is assumed to be continuous across the sheath in the collisionless model. The ion density and the ion velocity at the sheath edge are n_{i0} and v_0 respectively, and the positive-ion density n_i in the sheath is

$$n_i(V) = n_{i0}\left(1 + \frac{V}{V_0}\right)^{-1/2}. \tag{2}$$

The density of plasma electrons $n_e(V)$ is assumed to obey the Boltzmann distribution, so that

$$n_e(V) = n_{e0}\exp\left(-\frac{eV}{\kappa T_e}\right), \tag{3}$$

where n_{e0} is the density of electrons at the sheath edge, where we set $V = 0$. This relation is nearly exact if the potential of the electrode is much deeper than $\kappa T_e/e$. The density of negative ions $n_n(V)$ is also assumed to obey the Boltzmann distribution, so that

$$n_n(V) = n_{n0}\exp\left(-\frac{eV}{\kappa T_n}\right), \tag{4}$$

https://doi.org/10.1017/S0022377898006837 Published online by Cambridge University Press

where n_{n0} is the density of negative ions at the sheath edge, where we set $V = 0$. This is true for the case of $V_c \gg \kappa T_n/e$.

Poisson's equation in the sheath is

$$\varepsilon_0 \frac{\partial^2 V}{\partial x^2} = \rho, \tag{5}$$

where ε_0 is the dielectric constant in vacuum and ρ is the space charge density in the sheath. The latter is given by

$$\rho = \frac{en_{i0}}{(1+V/V_0)^{1/2}} - \frac{j_b(m/2e)^{1/2}}{(V_c - V)^{1/2}} - en_{e0}\exp\left(-\frac{eV}{kT_e}\right) - en_{n0}\exp\left(-\frac{eV}{kT_n}\right). \tag{6}$$

The following normalizations are made: the normalized potential $\eta = eV/\kappa T_e$; the normalized positive-ion density at the plasma boundary $\nu_i = n_{i0}/n_{e0}$; the normalized beam-current density $J_b = j_b/j_c$, where

$$j_c = n_{e0}\, e\left(\frac{\kappa T_e}{m}\right)^{1/2} (2\eta_c)^{3/2}; \tag{7}$$

the normalized negative-ion density at the plasma boundary $\nu_n = n_{n0}/n_{e0}$; the normalized distance from the cathode $\xi = x/\lambda_D$, where $\lambda_D = (\varepsilon_0 \kappa T_e/n_{e0} e^2)^{1/2}$ is the Debye length. Then the normalized Poisson's equation becomes

$$\frac{\partial^2 \eta}{\partial \xi^2} = \rho_n = \frac{\nu_i}{(1+\eta/\eta_0)^{1/2}} - \frac{J_b\,(2\eta_c)^{3/2}}{(2\eta_c - 2\eta)^{1/2}} - e^{-\eta} - \nu_n\, e^{-\gamma\eta} \tag{8}$$

where we define $\gamma = T_e/T_n$.

The boundary conditions are set as follows.

Quasineutrality is assumed at the sheath edge $\eta = 0$:

$$\nu_i = 1 + 2\eta_c\, J_b + \nu_n. \tag{9}$$

The derivative of the space charge density is assumed to be zero at $\eta = 0$:

$$\frac{\partial \rho_n}{\partial \eta} = 0 \quad \text{at} \quad \eta = 0. \tag{10}$$

Since, from (8),

$$\frac{\partial \rho_n}{\partial \eta} = -\frac{\nu_i/\eta_0}{2(1+\eta/\eta_0)^{3/2}} - \frac{J_b(2\eta_c)^{3/2}}{(2\eta_c - 2\eta)^{3/2}} + e^{-\eta} + \nu_n\, \gamma e^{-\gamma\eta} = 0, \tag{11}$$

we obtain

$$\eta_0 = \frac{1}{2}\frac{\nu_i}{1 - J_b + \nu_n\,\gamma} = \frac{1}{2}\frac{1 + 2\eta_c J_b + \nu_n}{1 - J_b + \nu_n\,\gamma}. \tag{12}$$

This agrees with the result for $J_b = 0$, $\nu_n = 0$ obtained by Bohm (1949). For $J_b = 0$, $\nu_n \neq 0$, it reduces to the result for the one-dimensional case (Boyd and Thompson 1959; Braithwaite and Allen 1988). The second of these papers also considers the spherical case.

The electron beam increases η_0 while the presence of negative ions decreases η_0 if $\gamma > 1$. Their effects balance each other to keep $\eta_0 = \frac{1}{2}$ when

$$(1 + 2\eta_c)\, J_b = (\gamma - 1)\, \nu_n. \tag{13}$$

https://doi.org/10.1017/S0022377898006837 Published online by Cambridge University Press

Zero electric field is assumed at the plasma–sheath boundary: $d\eta/d\xi = 0$ at $\eta = 0$. Integrating (8) with this boundary condition, we obtain

$$\tfrac{1}{2}E^2 = 2\nu_i\,\eta_0\left[\left(1+\frac{\eta}{\eta_0}\right)^{1/2}-1\right]-J_b(2\eta_c)^{3/2}[(2\eta_c)^{1/2}-(2\eta_c-2\eta)^{1/2}]$$

$$+e^{-\eta}-1+\frac{\nu_n}{\gamma}(e^{-\gamma\eta}-1). \quad (14)$$

The Maxwell stress at the cathode is given by $\eta = \eta_c$:

$$\tfrac{1}{2}E_c^2 = 2\nu_i\,\eta_0\left[\left(1+\frac{\eta_c}{\eta_0}\right)^{1/2}-1\right]-J_b\,(2\eta_c)^2+e^{-\eta_c}-1+\frac{\nu_n}{\gamma}(e^{-\gamma\eta_c}-1). \quad (15)$$

The maximum permitted beam current $J_{b\max}$ above which a virtual cathode appears is given, by putting $E_c^2 = 0$, as

$$J_{b\max} = \left\{2\nu_i\,\eta_0\left[\left(1+\frac{\eta_c}{\eta_0}\right)^{1/2}-1\right]+e^{-\eta_c}-1+\frac{\nu_n}{\gamma}(e^{-\gamma\eta_c}-1)\right\}\Big/(2\eta_c)^2. \quad (16)$$

Since ν_i and η_0 are functions of J_b as given by (9) and (12), $J_{b\max}$ can only be found numerically.

The normalized positive-ion current density $J_i = en_{i0}\,v_0/j_c$, using (7), is given by

$$J_i = \frac{\nu_i(2\eta_0)^{1/2}(m/M)^{1/2}}{(2\eta_c)^{3/2}}. \quad (17)$$

The ratio of positive-ion current to beam-electron current is found to be

$$\frac{J_i}{J_b} = \left(\frac{m}{M}\right)^{1/2}\frac{(1+2\eta_c J_b+\nu_n)^{3/2}}{J_b(1-J_b+\nu_n\,\gamma)^{1/2}(2\eta_c)^{3/2}}, \quad (18)$$

using (9) and (12).

3. Result of the calculations

The effect of negative ions has been investigated for the case without the beam ($J_b = 0$), to compare the space charge density, electric field and potential distributions with those of the previous case without negative ions (Prewett and Allen 1976).

First, the normalized potential was calculated numerically using the Runge–Kutta method, starting with the boundary conditions at $\eta = \eta_c$ and $d\eta/d\xi = -E_c$ at $\xi = 0$, and progressing ξ. At each step toward $\xi > 0$, a new η was substituted into E by using (14) to obtain a new $d\eta/d\xi$ and the normalized density ρ_n by using (8). As a typical value, $\eta_c = 10$ is taken according to Prewett and Allen (1976) for comparison.

It is assumed further that $\gamma = 10$ throughout this paper. The reason for the choice of this value is that in the case without a beam there is a critical value of γ, $\gamma_c = 5+\sqrt{24} = 9.899$, above which a multivalued solution is obtained, indicating a jump in η_0 (Braithwaite and Allen 1988). The multivalued solutions are known to exist for higher values in the case where there is no electron beam (Wickens and Allen 1979).

https://doi.org/10.1017/S0022377898006837 Published online by Cambridge University Press

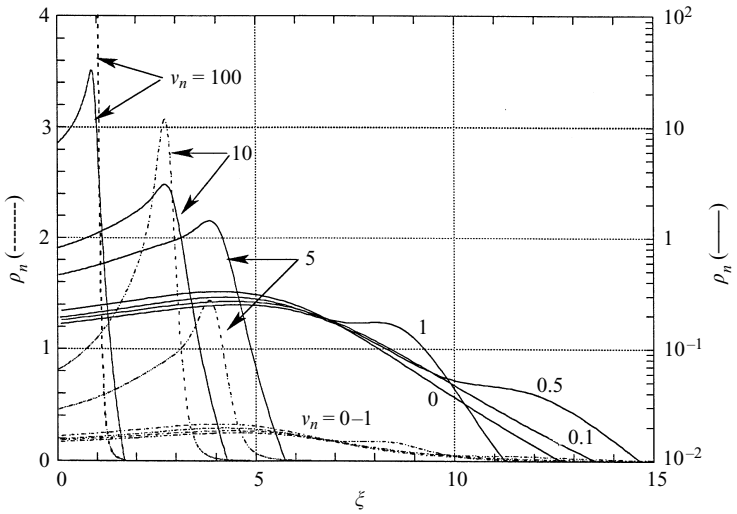


Figure 2. Spatial distribution of normalized space charge density ρ_n in the sheath with ν_n as a parameter ($J_b = 0$) for $\eta_c = 10$ and $\gamma = 10$.

Figure 2 shows the normalized space charge density ρ_n (the right-hand side of Poisson's equation (8)) for several values of ν_n, where $\xi = 0$ corresponds to the electrode. ρ_n is plotted on both logarithmic and linear scales in order to compare it with the case where an electron beam is present (Fig. 8). The assumption of Boltzmann distributions, (4) and (5), is valid because the inequalities $V_c \gg \kappa T_e/e$ and $V_c \gg \kappa T_n/e$ are fulfilled. The sheath becomes more ion-rich as ξ decreases, but there is a maximum of ρ_n (double humps for $\nu_n = 0.5$ and 1) at a certain position in the sheath. Very near the electrode ($\xi \approx 0$), ρ_n decreases from $\rho_n = 0.22$ for ($\nu_n = 0$) with increasing ν_n until $\nu_n \approx 0.5$, but begins to increase above $\nu_n = 1$. The sheath thickness x_s can be estimated from the value of $\xi = \xi_s$ at a small value of ρ_n, e.g. $\rho_n = 10^{-2}$, from $x_s = \xi_s (1+\nu_n)^{1/2}\lambda'_D$, where $\lambda'_D \equiv (\varepsilon_0 \kappa T_e/n_{i0} e^2)^{1/2}$. The factor $(1+\nu_n)^{1/2}$ means that charge neutralization by thermal electrons decreases owing to a decrease in the electron density. From the value of ξ at $\rho_n = 10^{-2}$, it is found that for small $\nu_n\,(< 0.1)$ and above $\nu_n = 5$, x_s always increases with ν_n for a given ion density. Although ξ at $\rho_n = 10^{-2}$ decreases from $\nu_n = 0.5$ to 5, this does not mean that x_s decreases by this amount, because the factor $(1+\nu_n)^{1/2}$ has to be taken into account.

The normalized electric field E was obtained for several values of ν_n. If the sheath thickness is defined at $\xi = \xi_s$, where $E = 10^{-3}$, the sheath thickness x_s increases from $\nu_n = 0$ to 0.1, but decreases slightly from $\nu_n = 0.1$ until $\nu_n = 1$, and then increases beyond $\nu_n = 1$. This is only slightly different from the x_s estimated from ρ_n. Instead of the factor 10^{-2} in the case of ρ_n, the selection of the factor 10^{-3} is only a problem of definition. It was selected to see the overall character of x_s. The sheath thickness depends on the definition. However, generally, it increases with ν_n at $\nu_n > 5$.

Figure 3 shows the normalized electric potential η obtained for several values of ν_n. The numerical calculation of the potential has been done for given η_c, γ and ν_n as follows. First, ν_i was calculated from (9) and η_c from (12). These were substituted into (15) to obtain E_c. By using the boundary conditions $\eta = \eta_c$ and $E = E_c$ at $\xi = 0$, $d\eta/d\xi$ was calculated by progressing ξ step by step. The

https://doi.org/10.1017/S0022377898006837 Published online by Cambridge University Press

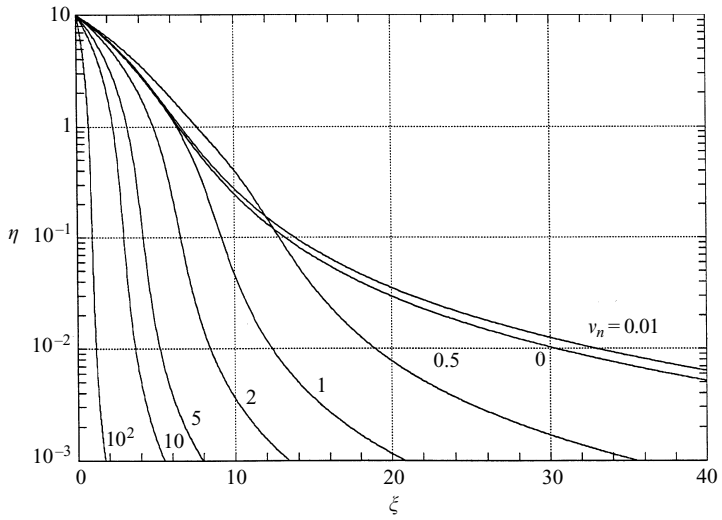


Figure 3. Spatial distribution of normalized electric potential η in the sheath with ν_n as a parameter ($J_b = 0$) for $\eta_c = 10$ and $\gamma = 10$.

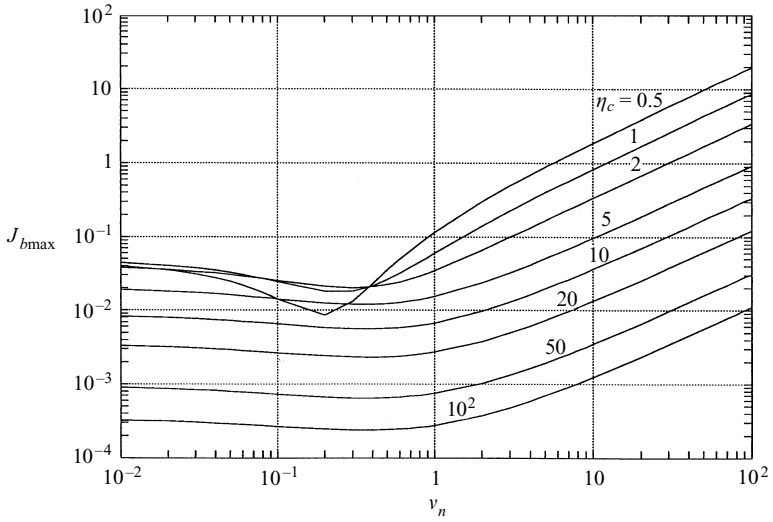


Figure 4. Maximum beam density $J_{b\max}$ above which a virtual cathode appears, as a function of ν_n for several values of η_c and $\gamma = 10$.

solution was obtained by checking that E increases or at least remains positive with increasing η, and $E \to 0$, $\eta \to 0$ at $\xi \to \infty$. The plot is shown for several values of ν_n except $\nu_n = 0.1$ (see the appendix). For the solutions that are obtained by satisfying the boundary conditions $\eta = \eta_c$ at $\xi = 0$ and $\eta = 0$ at $\xi \to \infty$, it may be seen that, in the presence of negative ions, if the sheath thickness is defined at $\xi = \xi_s$, where $\eta = 10^{-3}$ then similar properties are found to the case where E was considered.

Figure 4 shows the maximum beam density $J_{b\max}$ above which a virtual cathode appears, as a function of ν_n for several η_c. $J_{b\max}$ has been obtained by substituting η_0 given by the second equality in (12) into (16). At $\nu_n = 0$ and

https://doi.org/10.1017/S0022377898006837 Published online by Cambridge University Press

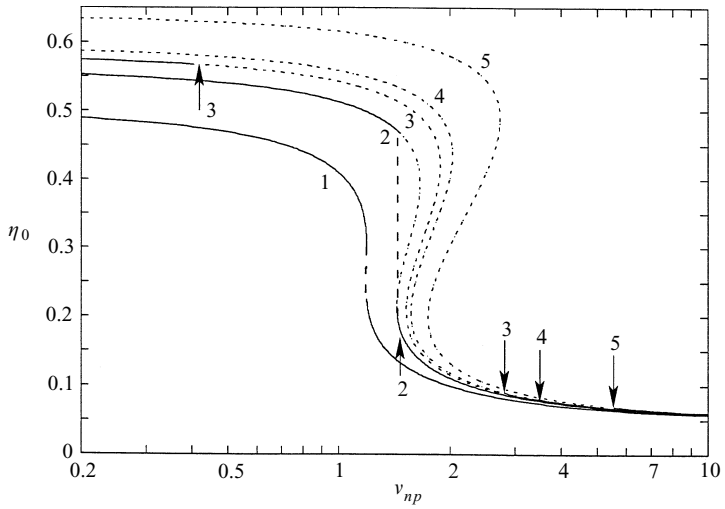


Figure 5. The initial ion energy η_0 as a function of ν_{np}, with J_b as a parameter ($\eta_c = 10$ and $\gamma = 10$). Curve 1, $J_b = 0$; curve 2, 5.62×10^{-3}; curve 3, 7.60×10^{-3}; curve 4, 8.73×10^{-3} ($= J_{b\max}$ for $\nu_{n0} = 0$), curve 5, 1.30×10^{-2}. Solid curves, allowable domains; dotted curves, disallowed domains. Jumps occur at $\nu_{np} = 1.19$ for curve 1 and at $\nu_{np} = 1.44$ for curve 2. Arrows 2–5 denote the terminal positions of the solid curves 2–5. Arrows terminate at $\nu_{np} = 0.40$ and 2.88 for curve 3, at $\nu_{np} = 3.35$ for curve 4 and at $\nu_{np} = 5.55$ for curve 5.

$\eta_c = 10$, we have $J_{b\max} = 0.008734$, as previously obtained by Prewett and Allen (1976). $J_{b\max}$ becomes smaller as η_c increases, except between $\nu_n = 0.01$ and 1. At a constant η_c, $J_{b\max}$ has a minimum between $\nu_n = 0.1$ and 1, and then increases almost linearly with ν_n above $\nu_n = 2$–3.

The initial ion energy η_0, which is equivalently a potential drop to the sheath edge to accelerate positive ions to form a stable sheath, was calculated from (12). For $\nu_n = 0$ and $J_b \to 0$, we have $\eta_0 = 0.5$ (Bohm 1949). η_0 decreases with ν_n; but at a constant ν_n, η_0 increases with J_b to a value limited by $J_{b\max}$. The condition (13) corresponding to the case where η_0 is kept at 0.5 is given by $J_b = \frac{3}{7}\nu_n$ for $\eta_c = 10$ and $\gamma = 10$. From (9), (12) and (16), this is possible only for $\nu_n \leqslant 0.018$.

Figure 5 shows η_0 as a function of the negative-ion to electron density ratio ν_{np} in the plasma far from the sheath. From the assumption of a Boltzmann distribution, $\nu_n = \nu_{np}\exp[(1-\gamma)\eta_0]$ is obtained. Putting this ν_n into (12), we obtain the relation between ν_{np} and η_0. In all the curves, η_0 decreases from $(1+2\eta_c J_b)/2(1-J_b)$ at $\nu_{np} = 0$ to $(2\gamma)^{-1}$ at $\nu_{np} \to \infty$. Curve 1 denotes the case $J_b = 0$ (Braithwaite and Allen 1988). Taking $\partial\nu_{np}/\partial\eta_0 = 0$, we find that between $\eta_0 = [1+\gamma \pm (\gamma^2 - 10\gamma + 1)^{1/2}]/4\gamma$, η_0 takes an inverted S shape (dashed curve) because of multiple values for a given ν_{np} (for $\gamma \leqslant \gamma_c$, η_0 takes a single value for a given ν_{np}). Therefore η_0 jumps from the lower branch to the higher branch drawn over the vertical dashed lines (the dashed curves and vertical dashed lines overlap owing to the narrow S shape). Curve 2 corresponds to the case of a finite J_b ($= 5.62 \times 10^{-3}$: the lowest value of $J_{b\max}$ in Fig. 4). Across the inverted S shape (dashed curve), η_0 jumps similarly to the higher branch as denoted by a vertical dashed line. All the values of $\nu_{np} > 0$ are allowable for curves 1 and 2 because the jumps occur vertically for these curves. However,

https://doi.org/10.1017/S0022377898006837 Published online by Cambridge University Press

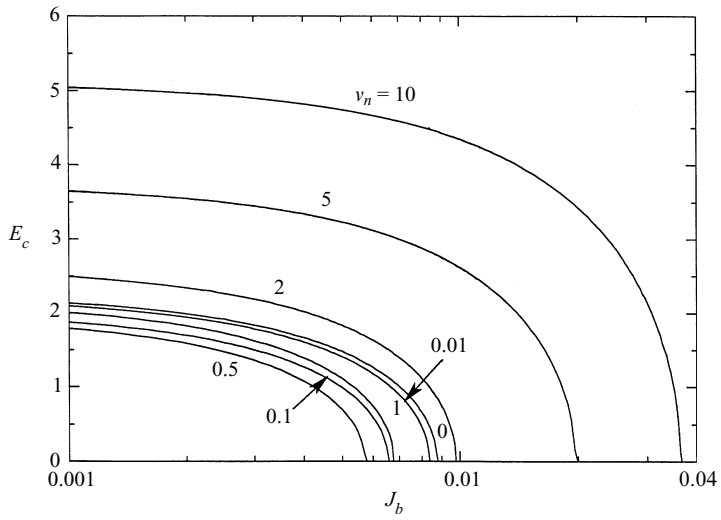


Figure 6. Normalized cathode electric field E_c as a function of J_b for $\eta_c = 10$ and $\gamma = 10$, with the negative-ion density ratio ν_n as a parameter.

for curves 3–5, only limited values of ν_{np}, as indicated by the solid curves, are allowable because of the limitation $J_b \leqslant J_{b\max}$. Curve 3 shows the case $J_b = 7.60 \times 10^{-3}$. In this case, only a part of the upper branch and a part of the lower branch away from the jump point are allowable (solid curves terminating at arrow 3). Curve 4 shows the case $J_b = 8.73 \times 10^{-3}$ ($J_{b\max}$ for $\nu_{np} = 0$), and curve 5 shows the case of a higher $J_b\,(= 1.30 \times 10^{-2})$. In the latter two cases, only parts of the lower branch away from the point of jump are allowable (solid curves starting from arrows 4 and 5), and other parts are inhibited (dashed parts).

Figure 6 shows the normalized electric field E_c at the electrode calculated from (15). At $\nu_n = 0$, E_c changes from 2.2727 at $J_b = 0$ to $E_c = 0$ at $J_b = J_{b\max} = 0.0087344$, which corresponds to the previous case without negative ions (Prewett and Allen 1976). For each value of ν_n, E_c decreases with J_b, and finally becomes zero at $J_b = J_{b\max}$ given in Fig. 4. E_c and $J_{b\max}$ decrease with ν_n from $\nu_n = 0$ to 0.5, but begin to increase with ν_n above $\nu_n = 0.5$.

Figure 7 shows the ratio of the positive-ion current J_i to the beam current J_b calculated from (18). For every ν_n, $(J_i/J_b)\ (M/m)^{1/2}$ decreases with J_b and terminates at $J_{b\max}$ before it approaches the limit of unity. As ν_n is increased from $\nu_n = 0$ to about 0.5, $(J_i/J_b)\ (M/m)^{1/2}$ decreases more with J_b than in the case of $\nu_n = 0$, but then begins to increase with ν_n. At higher ν_n ($\nu_n > 2$), $(J_i/J_b)\,(M/m)^{1/2}$ increases with increasing ν_n. It is of interest to compare the results with the well-known Langmuir limit $(J_i/J_b)(M/m)^{1/2} = 1$. This limit is for the case of two sets of particles only, each set having zero initial velocities (Langmuir 1929).

The effects of negative ions together with a beam will be described below in comparison with the case without negative ions (Prewett and Allen 1976). The numerical procedure is the same as in Figs 2 and 3.

Figure 8 shows the spatial distribution of ρ_n versus ξ for $\nu_n = 10$, with J_b as a parameter. The case $J_b = 0$ has already been given in Fig. 2. There is a

https://doi.org/10.1017/S0022377898006837 Published online by Cambridge University Press

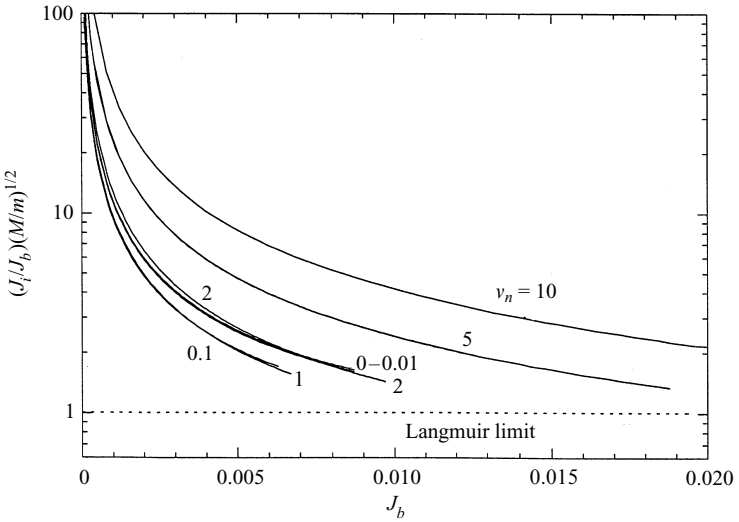


Figure 7. The ratio $(M/m)^{1/2}\, J_i/J_b$ as a function of J_b, with ν_n as a parameter for $\eta_c = 10$ and $\gamma = 10$. The line $(M/m)^{1/2} J_i/J_b = 1$ denotes the Langmuir limit. Each curve terminates at $J_b = J_{b\max}$ as given in Fig. 4. $J_{b\max} = 0.00873$ for $\nu_n = 0$, 0.00835 for $\nu_n = 0.01$, 0.00656 for $\nu_n = 0.1$, 0.00978 for $\nu_n = 2$, 0.0196 for $\nu_n = 5$, and 0.0364 for $\nu_n = 10$.

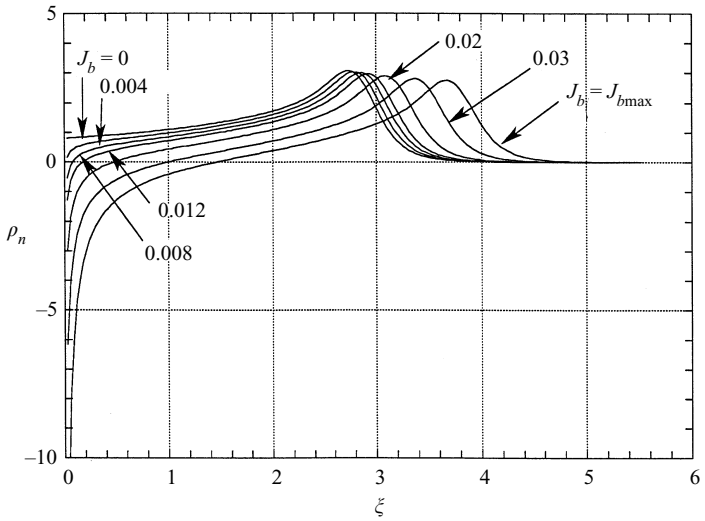


Figure 8. Spatial distribution of normalized space-charge density ρ in the sheath, with J_b as a parameter, for $\nu_n = 10$, $\eta_c = 10$ and $\gamma = 10$.

maximum of ρ_n at $\xi = 2.5$–4, and this maximum shifts to a higher ξ as J_b is increased. At the electrode ($\xi = 0$), ρ_n decreases with J_b toward negative values. This tendency is similar to the case without negative ions, except that ρ_n is smaller.

The spatial distribution of E versus ξ for $\nu_n = 10$, with J_b as a parameter, shows that the sheath thickness extends more as J_b is increased. At the electrode ($\xi = 0$), E decreases as J_b is increased, and the virtual-cathode condition is approached.

https://doi.org/10.1017/S0022377898006837 Published online by Cambridge University Press

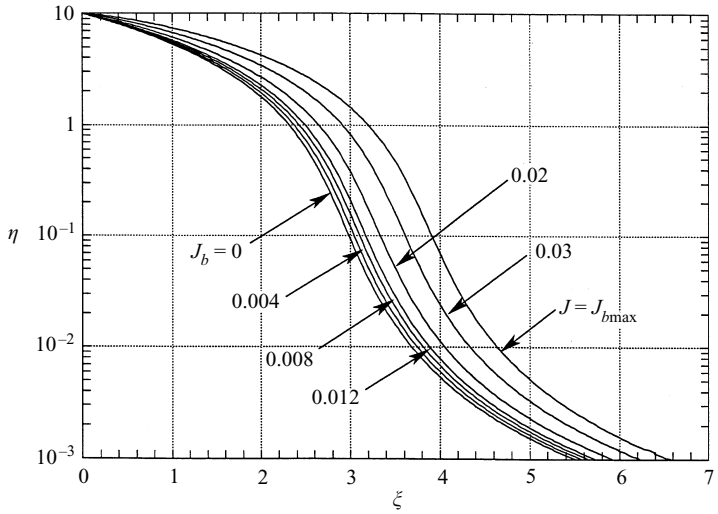


Figure 9. Spatial distribution of normalized electric potential η in the sheath, with J_b as a parameter, for $\nu_n = 10$, $\eta_c = 10$ and $\gamma = 10$.

Figure 9 shows the spatial distribution of η versus ξ for $\nu_n = 10$ for several values of J_b. The sheath thickness increases with J_b as in the case $\nu_n = 0$. Although the value of ξ is reduced to smaller values compared with the case $\nu_n = 0$, this does not necessarily indicate that the sheath thickness is smaller. The thickness should be considered to be the value of ξ at a smaller value of η (e.g. 10^{-3}) increased by a factor of $(1+\nu_n)^{1/2}$.

All the calculations given above are for a fixed value of η_c. Sometimes, however, the electrode is floated, as in the case treated by Hobbs and Wesson (1967). The model can be extended to obtain the floating potential of the emitting electrode. At the floating electrode, the current due to the positive ions and the beam is balanced by those of the thermal electrons, j_e, and of the negative ions, j_n. The last two currents are expressed in normalized units as

$$J_e = \frac{\exp(-\eta_c)}{(2\pi)^{1/2}(2\eta_c)^{3/2}}, \tag{19}$$

$$J_n = \nu_n\left(\frac{m}{M_n}\right)^{1/2}\frac{\exp(-\gamma\eta_c)}{(2\pi)^{1/2}(2\eta_c)^{3/2}}, \tag{20}$$

where M_n is the negative-ion mass.

If we consider the case where $\gamma > 1$ and $M_n \gg m$, we may assume that the negative-ion current is very small. Negative ions only influence the sheath edge potential and charge neutrality, and the current balance is given approximately by

$$J_i + J_b = J_e. \tag{21}$$

Introducing Γ as in the case of secondary emission (Hobbs and Wesson 1967),

$$J_b = \Gamma J_e, \quad \Gamma < 1, \tag{22}$$

but without specifying the emission process, we obtain from (17)

$$\exp(-\eta_c) = \left(\frac{2\pi m}{M}\right)^{1/2}\frac{\nu_i\,(2\eta_0)^{1/2}}{1-\Gamma}. \tag{23}$$

https://doi.org/10.1017/S0022377898006837 Published online by Cambridge University Press

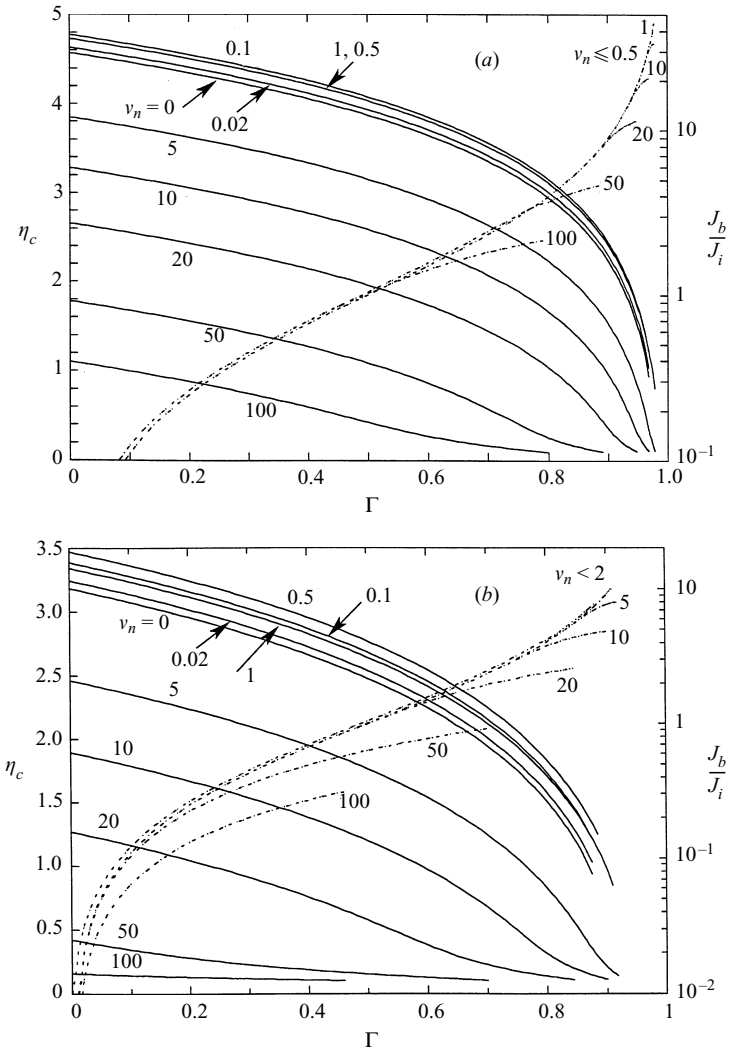


Figure 10. Normalized floating potential η_c as a function of Γ for several values of ν_n for (*a*) an O_2^-/O_2^+ plasma and (*b*) an H^-/H_2^+ plasma. In both (*a*) and (*b*), dotted curves indicate J_b/J_i. $\gamma = 10$.

If J_b and ν_n are small, we have $\eta_0 \approx 0.5$ and $2\eta_c J_b \ll 1$. Then (23) and (9) give

$$\eta_c \approx \frac{1}{2}\ln\left(\frac{M}{2\pi m}\right) - \ln\left(\frac{1}{1-\Gamma}\right) - \ln(1+\nu_n). \tag{24}$$

The first term is the usual floating potential without the beam and the negative ions. The second term is the modification due to the electron beam, and the third term is due to negative ions. Both lead to a decrease in η_c.

While ν_n is small (< 1), η_c from (24) is a good approximation. As ν_n becomes larger, the contribution of J_n is no longer negligible, and furthermore the positive ion current decreases with ν_n. In order to obtain η_c more accurately, the rigorous relation

$$J_i + J_b = J_e + J_n \tag{25}$$

https://doi.org/10.1017/S0022377898006837 Published online by Cambridge University Press

has been solved numerically using (24) to obtain an initial estimate.

Figure 10 (*a*) shows the normalized floating potential η_c and J_b/J_i as functions of Γ for some values of ν_n for the case with $M/m = M_n/m = 1836 \times 32$, the positive and negative ions being O_2^+ and O_2^- respectively. The calculation is stopped at $J_b = J_{b\max}$, where a virtual cathode appears. It can be seen that at a constant ν_n, η_c decreases with increasing Γ towards a small value (plasma boundary potential) and J_b/J_i increases with Γ. The increase in J_b becomes more remarkable as η_c approaches zero. Before η_c reaches a very small value near zero, however, the virtual-cathode condition is met. Except at small values of $\nu_n < 1$, where some crossings of η_c appear, η_c decreases with increasing ν_n. The reference of the potential is here the plasma boundary. As seen in Fig. 5, the potential at this boundary is lower than the maximum space potential by η_0. Therefore the absolute floating potential difference with respect to the maximum space potential is given by $\eta_c + \eta_0$. Figure 10 (*b*) shows the normalized floating potential η_c for the case with $M/m = 1836 \times 2$ and $M_n/m = 1836$, the positive and negative ions being H_2^+ and H^- respectively. Similar characteristics are obtained, but compared with the case of the heavier gas, η_c is larger and J_b/J_i is smaller.

5. Discussion

In the above calculations, only the case with $\eta_c = 10$ and $\gamma = 10$ has been treated. However, the present model can be readily applied to other cases.

As one application, in a H^- ion source, where extraction is made difficult by the ion sheath, secondary or electron emission from the electrode can help to raise the electrode potential with respect to the plasma potential and facilitate the extraction of negative ions. Since it was assumed above that $j_b < j_{b\max}$ and $\Gamma < 1$, the space potential could not be reached. The opposite case, namely that with injection of a beam from the plasma side, has been dealt with by Ingram and Braithwaite (1990), and this method has been found to be useful for controlling the electrode potential towards a negative bias (Bradley and Amemiya 1994) by using a beam with a very small density and a finite energy width.

Finally, it should be mentioned that much of the present work is applicable to the case of a plasma with two groups of electrons with different temperatures. Except for the current flowing to the electrode and the floating potential, most of the calculations do not depend on M_n. One example is recent work concerning space-charge layers in a double-plasma machine (Hassall and Allen 1997), where a double layer formed by source and target plasmas consisting of both cold and hot electrons has been considered.

6. Conclusions

The double-sheath theory has been considered for the case of emission of an electron beam from an electrode in a plasma containing negative ions. Some numerical results have been given for the space charge, electric field and the potential in the sheath in comparison with those of the case without negative ions. The floating potential has been obtained as a function of the negative-ion density ratio: the associated beam-density ratio has also been determined. The

https://doi.org/10.1017/S0022377898006837 Published online by Cambridge University Press

results can be applied to the control of the substrate potential in processing plasmas and also to the extraction of negative ions from negative-ion sources.

Acknowledgements

One of the authors (H. A.) thanks the Royal Society of London and the Japan Society for the Promotion of Science, Tokyo for giving him a chance to work in the Department of Engineering Science, Oxford in 1996.

Appendix

In the numerical calculation of the potential as shown in Fig. 3, for some particular cases around $\nu_n = 0.1$, it was found that while progressing the step, $E = 0$ occurs at values other than $\eta = 0$ (e.g. at $\eta = 0.083$), although $E \to 0$ as $\xi \to \infty$; that is, the sheath extends to large distances. This happens for a limited number of combinations of η_c, γ and ν_n. There are one or two points where E becomes zero as well as at $\eta = 0$. For the case of $\eta_c = 10$ and $\gamma = 10$, $\frac{1}{2}E^2$ in (14) becomes zero or negative at small $\eta (= 0\text{–}0.14)$ when $0.0818 < \nu_n < 0.145$. For such values of ν_n, mathematically exact solutions satisfying the boundary conditions were not obtained, although the ultimate value of η was small.

References

Andrews, J. G. and Allen, J. E. 1971 *Proc. R. Soc. Lond* **A320**, 459.

Bohm, D. 1949 *Characteristics of Electrical Discharges in Magnetic Fields* (ed. A. Guthrie and R. K. Wakerling), Chap. 3. McGraw-Hill, New York.

Boyd, R. L. F. and Thompson, J. B. 1959 *Proc. R. Soc. Lond.* **252**, 102.

Bradley, J. W. and Amemiya, H. 1994 *J. Phys. Soc. Japan* **63**, 3295.

Braithwaite, N. St. J. and Allen, J. E. 1988 *J. Phys.* **D21**, 1733.

Hassall, G. and Allen, J. E. 1997 *J. Phys.* **D30**, 381.

Hobbs, G. D. and Wesson, J. A. 1967 *Plasma Phys.* **9**, 85.

Ingram, S. G. and Braithwaite, N. St. J. 1990 *J. Phys.* **D23**, 1648.

Langmuir, I. 1929 *Phys. Rev.* **33**, 954.

Levine, J. S. and Crawford, F. W. 1980 *J. Plasma Phys.* **23**, 223.

Prewett, P. D. and Allen, J. E. 1976 *Proc. R. Soc. Lond.* **A348**, 435.

Wickens, L. M. and Allen, J. E. 1979 *J. Plasma Phys.* **22**, 167.

https://doi.org/10.1017/S0022377898006837 Published online by Cambridge University Press